Finite elements modelling of the long term behaviour of a full scale flexible pavement with the shakedown theory

Cyrille Chazallon, Fatima Allou, Pierre Hornych, Saida Mouhoubi

Finite elements modelling of the long-term behaviour of a full-scale flexible pavement with the shakedown theory

Cyrille Chazallon[1,*,†], Fatima Allou[2], Pierre Hornych[3] and Saida Mouhoubi[1]

[1]*Laboratory of Design Engineering, Institut National des Sciences Appliquées de Strasbourg, 24 Boulevard de la Victoire, 67084 Strasbourg Cedex, France*
[2]*Laboratory of Mechanics and Modelling of Materials and Structures in Civil Engineering, University of Limoges, Boulevard Derche, 19300 Egletons, France*
[3]*Materials and Pavements Structures Division, Laboratoire Central des Ponts et Chaussées, Route de Bouaye BP4129, 44341 Bouguenais Cedex, France*

Rutting, due to permanent deformations of unbound materials, is one of the principal damage modes of low-traffic pavements. Flexible pavement design methods remain empirical; they do not take into account the inelastic behaviour of pavement materials and do not predict the rutting under cyclic loading. A simplified method, based on the concept of the shakedown theory developed by Zarka for metallic structures under cyclic loadings, has been used to estimate the permanent deformations of unbound granular materials subjected to traffic loading. Based on repeated load triaxial tests, a general procedure has been developed for the determination of the material parameters of the constitutive model. Finally, the results of a finite elements modelling of the long-term behaviour of a flexible pavement with the simplified method are presented and compared with the results of a full-scale flexible pavement experiment performed by Laboratoire Central des Ponts et Chaussées. Finally, the calculation of the rut depth evolution with time is carried out.

KEY WORDS: elasto-plasticity; elastic shakedown; plastic shakedown; repeated load triaxial tests; full scale experiment

1. INTRODUCTION

Design and maintenance procedures for transportation infrastructures such as road pavements, railway track platforms and airfield pavements are aimed at assessing the permanent deformations of the bound or unbound layers. Low-traffic road pavements with a thin bituminous surfacing

*Correspondence to: Cyrille Chazallon, Laboratory of Design Engineering, Institut National des Sciences Appliquées de Strasbourg, 24 Boulevard de la Victoire, 67084 Strasbourg Cedex, France.
†E-mail: cyrille.chazallon@insa-strasbourg.fr

and granular base and subbase layers represent, in France, about 60% of the road network. In these pavements, permanent deformations of the unbound layers and of the soil represent the main cause of distress, leading to rutting of the pavement surface. Most of the current pavement design methods, used in pavement mechanics, are based on the so-called mechanistic empirical pavement analysis. Such approaches consist in calculating the response of the pavement using multi-layer linear elastic models and then comparing the calculated stresses or strains with empirical design criteria. Two criteria are generally used: a fatigue criterion for the asphalt layer based on the maximum tensile strain at the bottom of the asphalt layer and a rutting criterion for the subgrade soil, which consists in limiting the vertical elastic strains at the top of the subgrade. No model is used to predict the permanent deformations due to cyclic loading, and no design criterion is generally applied for the unbound granular layers.

In addition, design calculations are generally performed with fixed values of load, temperature and moisture conditions. In reality, low-traffic pavements are subjected to variable thermal, hydric and mechanical loadings, which have a strong influence on their behaviour, and a full modelling of these various coupled aspects has never been achieved yet.

The objective of this work is to improve the modelling of rutting of unbound pavement layers (granular layers and subgrades), for low-traffic pavements, with unbound granular bases. Field observations show that on such pavements, deterioration is mainly due to accumulation of permanent deformations in the unbound layers and that fatigue or cracking of the thin bituminous wearing course generally appears much later, when significant rutting has already developed. Therefore, in this work, deterioration of the bituminous layers due to fatigue or damage is not considered, and these layers are described using only visco-elastic models.

In soil mechanics, many elasto-plastic models have been developed for sands and clays, with isotropic or anisotropic hardening and kinematic hardening. The model simulations, which are the closest to the mechanical behaviour observed in pavements, are the models developed for earthquake applications. However, an important difference is the number of load cycles to simulate. Although the accelerogram of an earthquake represents about 100 loads cycles, the behaviour of flexible pavements has to be predicted for about 10^5–10^6 cycles, depending on the traffic, and in this case the vertical plastic strain is of prime importance. The use of such existing elasto-plastic models for pavement applications is difficult and leads to unrealistically high levels of plastic strains when very large numbers of load cycles are simulated [1].

To the authors' knowledge, permanent deformations of unbound granular materials (UGMs) for roads under large numbers of load cycles have been modelled using the following:

- *Analytical models*: Most of them have been listed by Lekarp and Dawson [2].
- *Plasticity-theory-based models*: They require the definition of a yield surface, plastic potential, isotropic hardening laws, and simplified accumulation rules [3, 4], or kinematic hardening laws [5].
- *Visco-plastic equivalent models*: They are based on the equivalence time, number of cycles, and have been developed by Suiker and de Borst [6] for the finite element modelling of a railway track platform and by Mayoraz [7] for the laboratory study of a sand.
- *Shakedown models*: These models are based on the concepts of the shakedown theory [8], used for metallic structures [9] and have been recently developed to determine the mechanical behaviour of UGMs under repeated loadings, typically repeated load triaxial tests [10–12].

Recently, the authors have developed a model based on the shakedown theory to predict permanent deformations of unbound granular layers in pavements [10]. In this paper, an improved version

of this model is presented and applied to predict the results of a full-scale experiment on a flexible pavement. This experiment has been performed on the accelerated pavement testing facility of Laboratoire Central des Ponts et Chaussées (LCPC, Nantes, France), in collaboration with the French Road Directorate. The model parameters are all determined from laboratory tests performed on the pavement materials [13].

The proposed model is based on the theory developed by Zarka and Casier [9] for metallic structures submitted to cyclic loadings. Zarka defines the plastic strains at elastic shakedown with Melan's static theorem [14] extended to kinematic hardening materials [15, 16]. The evaluation of the plastic strains in the pavement, when plastic shakedown occurs, is based on this simplified method. Chazallon and co-workers have extended the previous results to UGMs using the yield surface of Drucker–Prager [10]. Then, in order to describe the time-dependent evolution of the plastic strains accumulation, a parameter linking time and the number of cycles has been added [12].

To perform the 3D finite element modelling of the full-scale flexible pavement experiment, the model has been improved to take into account the initial state of the material, characterized by the following:

- the initial stress state [12];
- the initial water content;
- the initial anisotropy: the elasto-plastic calculation uses an orthotropic hyperelastic law.

The paper describes the new simplified model. Comparisons of model predictions with experimental results of cyclic triaxial tests on the materials from the LCPC full-scale-accelerated test are presented. Finally, the 3D finite element modelling of the full-scale experiment is carried out and compared with *in situ* measurements.

2. MODELS FOR PAVEMENT MATERIALS

Low-traffic pavements generally include a bituminous wearing course and unbound granular base and subbase layers. The hypotheses adopted in the finite element model for the various pavement materials are presented below.

Bituminous mixes are elasto-visco-plastic and thermo-sensitive materials. If, at low temperature they can be considered as purely elastic, in most usual conditions, their mechanical properties have to be determined over the range of conditions experienced *in situ*. Nevertheless, for low-traffic pavements, the contribution of the thin bituminous wearing course (typically 4–10 cm thick) to the overall rutting is rather low in comparison with that due to the unbound layers. For this last reason, in this work, the behaviour of this material will be considered visco-elastic. Linear visco-elastic models are usually used to describe the time-dependent and thermo-sensitive behaviour of this material. The behaviour of bitumen and asphalt mixtures can be described with a model made of series of many different Maxwell or Kelvin elements, which can be generalized by replacing the discrete elements by a continuous distribution of retardation times.

We will present in the following paragraphs another approach based on the bi-parabolic model of Huet [17] and Sayegh [18] and its calibration on complex modulus tests, which are the most appropriate tests for determining such material characteristics.

UGMs exhibit elasto-plastic behaviour without viscous dependency. Currently, in pavement research, their mechanical behaviour is studied with repeated load triaxial tests. These tests allow to study either the short-term resilient behaviour or the long-term behaviour where plastic strains

occur. The modified Boyce model developed in [19] is used to describe the short-term resilient behaviour, whereas the long-term behaviour is described by the shakedown model.

2.1. Bituminous materials

2.1.1. The Huet–Sayegh model. For the interpretation of complex modulus measurements, Huet [17] and Sayegh [18] have introduced in the year 1960 a constitutive law which, since then, has always been confirmed. From the representation of complex modulus (E^*) measurements in the classical Cole and Cole and Black planes, Huet and Sayegh proposed the following dependence of E^* with ω (pulse) and θ (temperature):

$$E^*(\omega\tau(\theta)) = E_0 + \frac{E_\infty - E_0}{1+\delta(\mathrm{i}\omega\tau(\theta))^{-k} + (\mathrm{i}\omega\tau(\theta))^{-h}} \tag{1}$$

with E_0 and E_∞ being limits of the complex modulus for $\omega = 0$ or $+\infty$; h and k being parameters such that $1 > h > k > 0$, related, respectively, to the ratio $E_{\mathrm{imag}}/E_{\mathrm{real}}$ when ω tends to 0 (respectively, to infinity) the δ one dimensionless constant; and $\tau(\theta)$ being a function of temperature, which accounts for the classical equivalence principle between frequency and temperature.

Huet and Sayegh have shown that their equation for the complex modulus corresponds to the analogical model of Figure 1 with two branches: one with a spring and two parabolic dashpots corresponding to instantaneous and delayed elasticity (branch I) and the other one with the spring $E_0 (\ll E_\infty)$ representing the static or long-term behaviour (branch II).

Huet and Sayegh suggested to approximate $\tau(\theta)$ by an Arrhenius- or Eyring-type law:

$$\tau(\theta) = A\exp(-B/T) \quad \text{with} \quad T = 273^\circ + \theta \tag{2}$$

where A and B are model parameters.

In fact, for the limited range of temperatures found in pavements, the following exponential-parabolic law is used here:

$$\tau(\theta) = \exp(A_0 + A_1\theta + A_2\theta^2) \tag{3}$$

where A_0, A_1 and A_2 are model parameters.

2.1.2. Adjustment of the model parameters. The model parameters can be easily determined from complex modulus tests. At LCPC, the complex modulus is determined from alternate flexural tests on trapezoïdal specimens, performed under imposed strain, for different values of frequency (1, 3, 10, 30, 40 Hz) and temperature ($-10, 0, 10, 20, 30, 40$°C). In this work, the Huet–Sayegh model

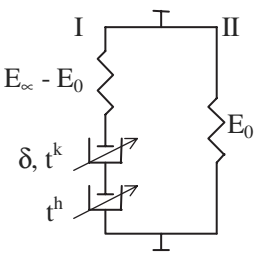

Figure 1. Analogical representation of the Huet and Sayegh model.

was used to model the bituminous material from the LCPC full-scale experiment. Figure 2 shows the prediction of the complex modulus values, in the Cole and Cole plane (E_{imag} *vs* E_{real}). The model parameters are given in Table I.

2.2. *Unbound materials*

Models for subgrades and unbound layers in pavements have been split into two categories, dealing with the short-term and the long-term behaviours:

- Resilient behaviour of UGMs for roads is studied by laboratory repeated load triaxial tests and generally modelled with non-linear elasticity [20]. This resilient behaviour is obtained in pavements when the granular base is adapted (elastic shakedown) or accommodated (plastic shakedown).
- Long-term elasto-plastic behaviour: these models are based on results of repeated load triaxial and monotonic triaxial tests.

2.2.1. The modified Boyce model. The model used to describe the elastic part of the behaviour of UGMs is a non-linear elastic model proposed by Boyce [21]. This model was first applied in France to the modelling of UGMs by Paute *et al.* [22] and was modified by Hornych *et al.* [19] to take into account anisotropy. This model is defined by the following stress–strain relationships:

$$\varepsilon_v^* = \frac{1}{K_a}\frac{p^{*n}}{p_a^{n-1}}\left[1+\frac{(n-1)K_a}{6G_a}\left(\frac{q^*}{p^*}\right)^2\right] \quad \text{and} \quad \varepsilon_q^* = \frac{1}{3G_a}\frac{p^{*n}}{p_a^{n-1}}\frac{q^*}{p^*} \tag{4}$$

with $p^* = (\gamma\sigma_1 + 2\sigma_3)/3$ and $q^* = \gamma\sigma_1 - \sigma_3$; $\varepsilon_v^* = \varepsilon_1/\gamma + 2\varepsilon_3$ and $\varepsilon_q^* = \frac{2}{3}(\varepsilon_1/\gamma - \varepsilon_3)$; K_a, G_a, n and γ are the parameters of the model.

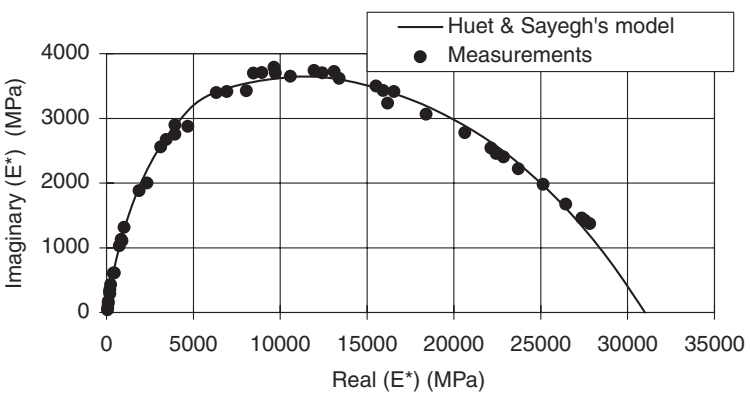

Figure 2. Adjustment of the complex modulus values of the bituminous material in Cole and Cole axes.

Table I. Huet–Sayegh parameters of the bituminous material.

E_0 (MPa)	E_{inf} (MPa)	K	h	Delta	A_0	A_1	A_2
37	31 000	0.254	0.76	2.48	2.374	−0.380	0.00251

In this work, a macroscopic cohesion parameter p^0 has been added to the expression of the mean stress p^* of the anisotropic Boyce model to take into account the cohesion due to the unsaturated state of the UGM. Thus, in the expression of the Boyce model, the stress value p^* has been replaced by the value: $p^+ = p^0 + p^*$.

We will present in the following paragraph the shakedown constitutive model for modelling of UGMs and present the modifications developed to take into account the initial anisotropy of the material.

3. THE SHAKEDOWN CONSTITUTIVE MODEL

Let us consider an elasto-plastic structure. Its boundary Γ is subjected to imposed surface forces $F_i^{\mathrm{d}}(x,t)$ in the Γ_{F_i} partition and to prescribed surface displacements $U_j^{\mathrm{d}}(x,t)$ in the Γ_{U_j} partition. x is the space coordinates vector. The body forces $X_j^{\mathrm{d}}(x,t)$ and the initial strain $\varepsilon_{ij}^{\mathrm{I}}(x,t=0)$ are defined in the volume V. This structure is supposed to satisfy the theory of small displacements and deformations. The general problem can be solved with the finite elements method as follows:

$$\varepsilon_{ij}(x,t) = M_{ijkl}\sigma_{kl}(x,t) + \varepsilon_{ij}^{\mathrm{p}}(x,t) + \varepsilon_{ij}^{\mathrm{I}}(x,0) \tag{5}$$

where the actual strain tensor $\varepsilon_{ij}(x,t)$ is kinematically admissible with $U_j^{\mathrm{d}}(x,t)$ on Γ_{U_j} and the actual stress tensor $\sigma_{ij}(x,t)$ is statically admissible with $F_i^{\mathrm{d}}(x,t)$ on Γ_{F_i} and with $X_j^{\mathrm{d}}(x,t)$ in V; $\varepsilon_{ij}^{\mathrm{p}}(x,t)$ is the plastic strain tensor; $\varepsilon_{ij}^{\mathrm{I}}(x,0)$ is the initial strain tensor and M_{ijkl} is the compliance linear elasticity matrix. The basic general problem can be decomposed into elastic and inelastic parts.

3.1. Elastic problem

The response associated with the elastic part is expressed as follows:

$$\varepsilon_{ij}^{\mathrm{el}}(x,t) = M_{ijkl}\sigma_{kl}^{\mathrm{el}}(x,t) + \varepsilon_{ij}^{\mathrm{I}}(x,0) \tag{6}$$

where the elastic strain tensor $\varepsilon_{ij}^{\mathrm{el}}(x,t)$ is kinematically admissible with $U_j^{\mathrm{d}}(x,t)$ on Γ_{U_j} and the elastic stress tensor $\sigma_{ij}^{\mathrm{el}}(x,t)$ is statically admissible with $F_i^{\mathrm{d}}(x,t)$ on Γ_{F_i} and with $X_j^{\mathrm{d}}(x,t)$ in V.

3.2. Inelastic problem

The inelastic problem is obtained by the difference between the total and the elastic problems. It can be expressed according to the following equation:

$$\varepsilon_{ij}^{\mathrm{ine}}(x,t) = \varepsilon_{ij}(x,t) - \varepsilon_{ij}^{\mathrm{el}}(x,t) = M_{ijkl}R_{kl}(x,t) + \varepsilon_{ij}^{\mathrm{p}}(x,t) \tag{7}$$

where $\varepsilon_{ij}^{\mathrm{ine}}(x,t)$ is kinematically admissible with 0 on Γ_{U_j}.

The residual stress field $R_{ij}(x,t)$ is obtained by the difference between the actual and the elastic stress fields as follows:

$$R_{ij}(x,t) = \sigma_{ij}(x,t) - \sigma_{ij}^{\mathrm{el}}(x,t) \tag{8}$$

It is statically admissible with 0 on Γ_{F_i} and with 0 in V.

With the knowledge of the plastic strain tensor $\varepsilon_{ij}^{\mathrm{p}}(x,t)$ and the compliance linear elasticity matrix M_{ijkl}, the inelastic problem is solved with a null stress boundary condition and the inelastic strain field $\varepsilon_{ij}^{\mathrm{ine}}(x,t)$ is obtained.

In the method developed by Zarka for metallic structures under large numbers of cycles, internal structural parameters are introduced to give an estimate of the stabilized state and the inelastic components. This method has been modified by Habiballah and Chazallon [10] to predict the inelastic behaviour of UGM under large numbers of cycles. The yield surface and plastic potential are composed of the Drucker–Prager yield surface, which defines the elastic domain ($r<r_{\min}$) and the Von Mises yield surface when plastic flow occurs $r\geqslant r_{\min}$ (Figure 3). A linear kinematic hardening is used for both. The expressions are the following:

$$f=\sqrt{\tfrac{1}{2}(S_{ij}-y_{ij})(S_{ij}-y_{ij})}-\alpha I_1(\sigma_{ij})-k \quad \text{if } \alpha I_1(\sigma_{ij})+k<r_{\min} \tag{9}$$

$$f=\sqrt{\tfrac{1}{2}(S_{ij}-y_{ij})(S_{ij}-y_{ij})}-r \quad \text{if } r\geqslant r_{\min} \tag{10}$$

where $r=\alpha I_1(\sigma_{ij})+k$, $y_{ij}=(2H/3)\varepsilon_{ij}^{\mathrm{p}}$ is the kinematic hardening tensor, H is the hardening modulus, S_{ij} is the deviatoric part of the actual stress tensor σ_{ij}, $I_1(\sigma_{ij})$ is the first stress invariant and α and k are material parameters.

The actual deviatoric stress can be expressed as

$$S_{ij}(x,t)=S_{ij}^{\mathrm{el}}(x,t)+\mathrm{dev}\,R_{ij}(x,t) \tag{11}$$

We define the structural transformed parameters field Y_{ij} by

$$Y_{ij}(x,t)=y_{ij}(x,t)-\mathrm{dev}\,R_{ij}(x,t) \tag{12}$$

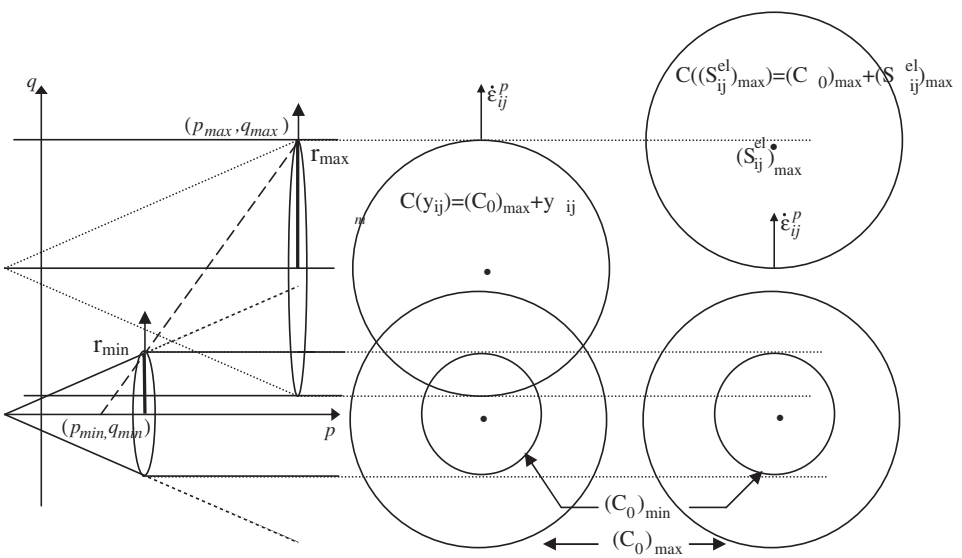

Figure 3. Evolution of plasticity criteria convex in the (p,q) plane, deviatoric plane and in the transformed structural parameters plane.

Then, substituting it in (9) and (10), the yield surface in the deviatoric plane can be expressed as follows:

$$f(S_{ij}^{\mathrm{el}} - Y_{ij}) \leqslant 0 \tag{13}$$

The yield surface boundary becomes a circle centred in S_{ij}^{el}, in the structural transformed parameters plane. The inelastic problem can be expressed with the structural transformed parameters field:

$$\varepsilon_{ij}^{\mathrm{ine}}(x,t) = M'_{ijkl} R_{kl}(x,t) + \frac{3}{2H} Y_{ij}(x,t) \tag{14}$$

where M'_{ijkl} is the modified linear elasticity matrix, defined by the following equality:

$$M'_{ijkl} = M_{ijkl} + \frac{3}{2H}\mathrm{dev} \tag{15}$$

3.3. Response of a structure subjected to a cyclic loading

During a cyclic loading, the elastic response of the structure can be expressed as

$$\sigma_{ij}^{\mathrm{el}}(x,t) = (1-\Lambda(t))\sigma_{ij_{\min}}^{\mathrm{el}}(x) + \Lambda(t)\sigma_{ij_{\max}}^{\mathrm{el}}(x) \tag{16}$$

where $\sigma_{ij_{\min}}^{\mathrm{el}}(x)$ and $\sigma_{ij_{\max}}^{\mathrm{el}}(x)$ are, respectively, the minimum and maximum values of the cyclic loading, and $\Lambda(t)$ is a periodic function of time.

The local stresses at the level of the plastic mechanisms are expressed as

$$\tilde{\sigma}_{ij}(x,t) = S_{ij}(x,t) - y_{ij}(x,t) \tag{17}$$

In the local stress plane, the plasticity convex domains $(C_0)_{\min}$ at the minimum stress state and $(C_0)_{\max}$ at the maximum stress state are fixed cones that are reduced, in the deviatoric plane, to circles centred on the isotropic stress axis (Figure 3). The normality law is expressed with Moreau's notation [23]:

$$\dot{\varepsilon}_{ij}^{\mathrm{p}} \in \partial\psi_{(C_0)_{\min}}(\tilde{\sigma}_{ij}) \quad \text{with } \tilde{\sigma}_{ij} \in (C_0)_{\min} \tag{18}$$

$\partial\psi_{(C_0)_{\min}}(\tilde{\sigma}_{ij})$ is the subdifferential to the convex $(C_0)_{\min}$ at $\tilde{\sigma}_{ij}$, where the plastic strain rate is an external normal to the convex $(C_0)_{\min}$.

At the maximum stress state and using (12), the transformed structural parameter at the level of the inelastic mechanism is

$$Y_{ij} = -\tilde{\sigma}_{ij} + S_{ij_{\max}}^{\mathrm{el}} \tag{19}$$

with $Y_{ij} \in C(S_{ij_{\max}}^{\mathrm{el}})$ and $C(S_{ij_{\max}}^{\mathrm{el}}) = (C_0)_{\max} + S_{ij_{\max}}^{\mathrm{el}}$.

Equation (19) implies that Y_{ij} belongs to the convex set $C(S_{ij_{\max}}^{\mathrm{el}})$ obtained from $(C_0)_{\max}$ with the translation $S_{ij_{\max}}^{\mathrm{el}}$ (Figure 3). The normality law is

$$\dot{\varepsilon}_{ij}^{\mathrm{p}} \in -\partial\psi_{C(S_{ij_{\max}}^{\mathrm{el}})}(Y_{ij}) \quad \text{with } Y_{ij} \in C(S_{ij_{\max}}^{\mathrm{el}}) \tag{20}$$

$-\partial\psi_{C_{(S_{ij_{\max}}^{\mathrm{el}})}}(Y_{ij})$ is the subdifferential to the convex $C(S_{ij_{\max}}^{\mathrm{el}})$ at $Y_{ij}(x,t)$, where the plastic strain rate is an internal normal to the convex $C(S_{ij_{\max}}^{\mathrm{el}})$. This convex is locally built for each

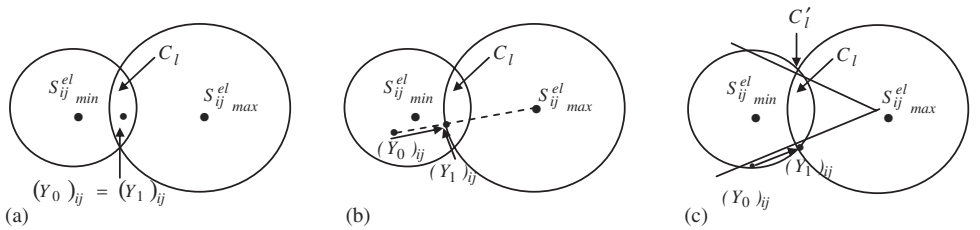

Figure 4. Cases to assess $(Y_1)_{ij}$.

plastic mechanism. Thus, in the transformed structural parameters plane, the yield surface is a circle centred in $S^{\mathrm{el}}_{ij_{\max}}(x,t)$.

The nature of the limit state of the structure will depend on the elastic response. According to the loading amplitude $\Delta S^{\mathrm{el}}_{ij}$, the convex set $C(S^{\mathrm{el}}_{ij}) = (C_0) + S^{\mathrm{el}}_{ij}$ moves linearly between $C(S^{\mathrm{el}}_{ij_{\min}})$ and $C(S^{\mathrm{el}}_{ij_{\max}})$. The following two situations exist:

- Elastic shakedown will occur when those two sets have a common part C_l.
- Otherwise, plastic shakedown occurs.

3.4. Elastic shakedown

At each point of a structure in an elastic shakedown situation, the initial structural transformed parameters $(Y_0)_{ij}$ are transported with the movement of the plastic convex. Three cases can be obtained:

- $(Y_0)_{ij}$ is inside C_l and remains immobile (Figure 4(a)).
- $(Y_0)_{ij}$ is such that, after the first cycle, it reaches the boundary of C_l and remains immobile (Figure 4(b)).
- $(Y_0)_{ij}$ is transported with the movements of the convex to finish on the boundary C_l or C'_l (Figure 4(c)). In this case, the stabilized state is reached after several cycles.

Thus, the new position $(Y_1)_{ij}$ determines the final cycle that solves the inelastic and the general problems.

3.5. Plastic shakedown

A lower bound solution is obtained from geometrical considerations [9]. In the structural transformed parameters plane, $Y_{ij_{\max}}$ and $Y_{ij_{\min}}$ belong to extreme positions of the two convexes centred in $S^{\mathrm{el}}_{ij_{\max}}$ and $S^{\mathrm{el}}_{ij_{\min}}$, respectively. The final cycle is defined by the mean value $(\varepsilon^{\mathrm{p}}_{ij})_{\mathrm{mean}}$ and the range $\Delta\varepsilon^{\mathrm{p}}_{ij}$. Thus, the values of the ΔY_{ij} and $(Y_{ij})_{\mathrm{mean}}$ fields are, respectively,

$$\Delta Y_{ij}(x) = \Delta S^{\mathrm{el}}_{ij}(x)\left(1 - \frac{r_{\min}(x) + r_{\max}(x)}{\sqrt{\frac{1}{2}(\Delta S^{\mathrm{el}}_{ij}(x)\Delta S^{\mathrm{el}}_{ij}(x))}}\right) \tag{21}$$

$$(Y_{ij})_{\mathrm{mean}}(x) = \frac{\Delta S^{\mathrm{el}}_{ij}(x)}{2}\left(1 + \frac{r_{\min}(x) - r_{\max}(x)}{\sqrt{\frac{1}{2}(\Delta S^{\mathrm{el}}_{ij}(x)\Delta S^{\mathrm{el}}_{ij}(x))}}\right) + S^{\mathrm{el}}_{ij_{\min}}(x) \tag{22}$$

where $r_{\min}$ and $r_{\max}$ are the radii of the two convexes centred in $S^{\mathrm{el}}_{ij_{\min}}$ and $S^{\mathrm{el}}_{ij_{\max}}$ (see Figure 5). Their values are

$$r_{\min}(x) = \alpha\sqrt{3}I_1(\sigma^{\mathrm{el}}_{ij_{\min}}(x)) + k\sqrt{3} \tag{23}$$

$$r_{\max}(x) = \alpha\sqrt{3I_1}(\sigma^{\mathrm{el}}_{ij_{\max}}(x)) + k\sqrt{3} \tag{24}$$

Modifications have been added in order to describe the accumulation of plastic strains with time. For that, a function $F(N)$ has been defined, which is applied:

- to the stabilized plastic deformations for modelling of repeated load triaxial tests, as follows (homogeneous test):

$$\overline{\varepsilon^{\mathrm{p}}_{ij}(x, N)} = F(N)(\varepsilon^{\mathrm{p}}_{ij\,\mathrm{mean}}(x) \pm \Delta\varepsilon^{\mathrm{p}}_{ij}(x)/2) \tag{25}$$

- to the stress state for finite elements modelling, since $\varepsilon^{\mathrm{ine}}_{ij}(x)$ is a function of $Y_{ij}(x)$ (11), which is expressed with $S^{\mathrm{el}}_{ij_{\min}}(x)$, $S^{\mathrm{el}}_{ij_{\max}}(x)$ and $\Delta S^{\mathrm{el}}_{ij}(x)$ (21), (22).

From repeated load triaxial tests, Hornych *et al.* [24] have proposed the following equation to relate permanent axial strains with the number of cycles:

$$\varepsilon^{\mathrm{p}}_1 = F(N) \cdot A \tag{26}$$

where

$$F(N) = \left[1 - \left(\frac{N}{100}\right)^{-B}\right] \tag{27}$$

$\varepsilon^{\mathrm{p}}_1$ is the vertical plastic strain; N is the number of cycles; A is the limit value of $\varepsilon^{\mathrm{p}}_1$ when N tends towards the infinite; B controls the shape of the plastic strains curve.

In the following paragraphs, we will present the identification of the model parameters.

3.6. Evaluation of model parameters

The simplified method requires the linear elasticity parameters, Drucker–Prager parameters (the elasticity cone aperture ψ and the apex of the Drucker–Prager cone on the isotropic stress axis p^*),

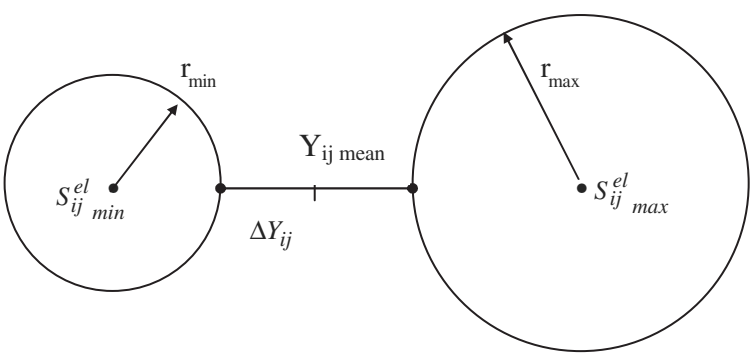

Figure 5. Value of $Y_{ij_{\mathrm{mean}}}$ and ΔY_{ij} during plastic shakedown.

the hardening modulus and the function $F(N)$. In order to determine the model parameters, monotonic and repeated load triaxial tests have been performed on the granular material (crushed gneiss (0/20 mm) from the Maraîchères quarry) [13]. The same approach has been carried out for the subgrade (Missillac sand), but the results will not be presented in detail.

The mechanical characteristics of these two materials are shown in Table II:

3.6.1. Drucker–Prager parameters. The parameter $p^* = k/3\alpha$ is the elasticity cone vertex position on the isotropic axis. It is identified by the failure line obtained from three monotonic triaxial tests. The parameter $\psi = \text{artg}(3\alpha\sqrt{3})$ represents the elasticity cone aperture in the (p, q) stress space. It is chosen to obtain a reduced initial elastic domain just before the plastic flow, where the elastic strain is equal to 10^{-5} for a low stress path ratio q/p. Representative Drucker–Prager parameters of the Maraîchères granular material are listed in Table III.

3.6.2. Determination of the elasticity parameters. The determination of the non-linear elastic model parameters is based on a cyclic triaxial test, where both the axial stress and the cell pressure are cycled. This test consists in applying to the specimen a series of 19 cyclic load sequences, following different stress paths, with different stress ratios $\Delta q/\Delta p$. The stress paths applied are shown in Figure 6.

The parameters of the model are determined using the resilient strains obtained for each cyclic loading (strains at unloading). An example of prediction of the resilient strains for a triaxial test on the Maraîchères material is shown in Figure 7, and the values of the corresponding non-linear elastic model parameters are given in Table IV.

3.6.3. Plasticity parameters. Two parameters are required: the hardening modulus H and the function $F(N)$. These two parameters require an adjustment on repeated load triaxial tests results, with different stress ratios. Two series of tests were conducted on the UGM (Maraîchères) and on the subgrade material (Missillac sand). We will present in this paper results obtained on the Maraîchères material (for a water content $w = 4\%$).

For the cyclic triaxial tests, a multi-stage test procedure developed by Gidel *et al.* [25] has been used. It consists, in each permanent deformation test, in performing successively several cyclic

Table II. Mechanical characteristics of the unbound granular material and subgrade soil.

Material	LA	MDE	Fines content (%)	ρ_{dSOP} (kg/m^3)	w_{SOP} (%)
Maraîchères	16	10	9	2170	6.3
Missillac	—	—	7.5	2040	9.2

LA, Los Angeles value; MDE, micro-Deval test; ρ_{dSOP} and w_{dSOP}, dry density and water content achieved at the standard optimum proctor test.

Table III. Parameters of the Drucker–Prager model.

Material	$\psi(^\circ)$	p^* (kPa)
Maraîchères (w = 4%)	15	40
Missillac ($w = 11\%$)	15	12.8

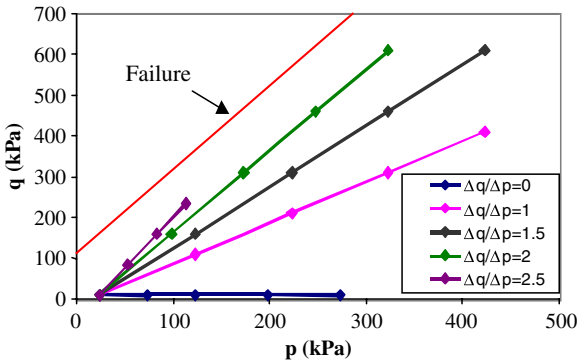

Figure 6. Cyclic loads applied during the resilient behaviour tests (Maraîchères material).

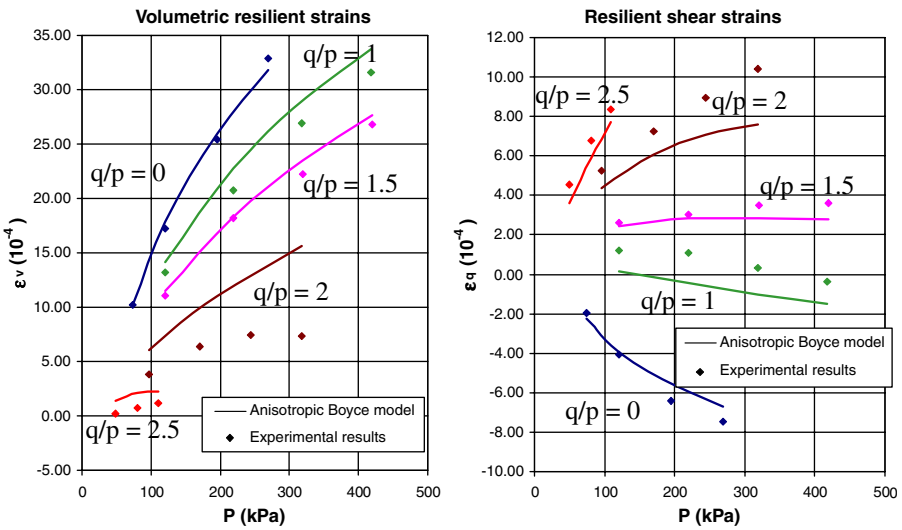

Figure 7. Prediction of the resilient behaviour with the anisotropic Boyce model (Maraîchères material).

Table IV. Parameters of the anisotropic Boyce Model.

	K_a (MPa)	G_a (MPa)	n	γ
Maraîchères ($w=4\%$)	7.1	27.4	0.16	0.45
Missillac ($w=11\%$)	22.9	31.7	0.54	0.64

load sequences, following the same stress path, with the same q/p ratio ($q/p=1$, 2 and 2.5 for the Maraîchères material) but with increasing stress amplitudes (Figure 8).

Each loading stage was applied for 50 000 cycles instead of 10 000 cycles for the Missillac sand in order to have a very low plastic strain rate at the end of each loading (around 10^{-8} per cycle) and

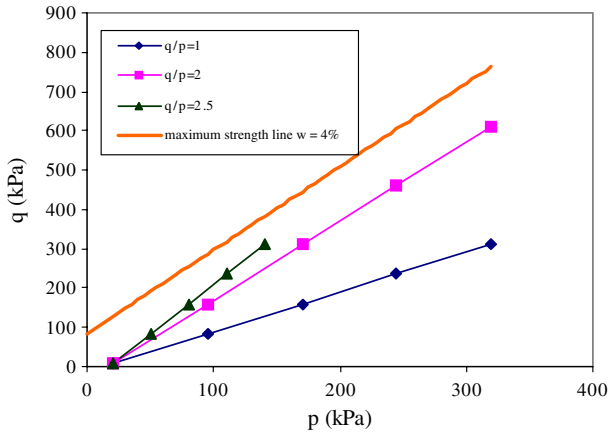

Figure 8. Cyclic loads applied during the staged loading tests (Maraîchères material).

allow a more accurate determination of the model parameters. The simplified elasto-plastic model is based on the shakedown theory and gives the stabilized plastic strains. Thus, the hardening modulus calibration has to be determined using limit state plastic strains (26).

With the corresponding stabilized plastic strains (26), elasticity and Drucker–Prager parameters, we determine the hardening modulus and parameter B, with the simplified method. We assume a linear evolution of the hardening modulus with the stress path length for each stress ratio (q/p), in the

$$\left(\mathrm{Log}\left[\frac{p_{\min}}{\Delta p}\right], \mathrm{Log}\left[\frac{H}{p_a}\cdot\frac{L_{\min}}{L}\right]\right)$$

plane (Figure 9), where $L_{\min}=\sqrt{p_{\min}^2+q_{\min}^2}$ and $L=\sqrt{\Delta p^2+\Delta q^2}$.

Thus, the hardening modulus is expressed hereafter as

$$H=10^b\cdot\frac{L}{L_{\min}}\cdot\left(\frac{p_{\min}}{\Delta p}\right)^a\cdot p_{\mathrm{a}} \tag{28}$$

where a and b are material parameters and p_{a} is the atmospheric pressure. Parameters a and b are determined with linear regressions, which are functions of the q/p ratio.

In (28), the hardening modulus is a function of the applied stress and of the initial stress state of the material. Its influence on the amount of vertical plastic strain is taken into account in the evolution law of 'a' and 'b' parameters by a bilinear function (Figure 10).

To estimate the rut depth evolution with time (number of cycles), we propose to use the previous approach to determine the evolution law of B. We assume a linear evolution of the B parameter with the stress path length, the applied stress and the initial stress state of the material for each stress ratio q/p, in the

$$\left(\left[\frac{p_{\min}}{\Delta p}\right], \left[B\cdot\frac{L_{\min}}{L}\right]\right)$$

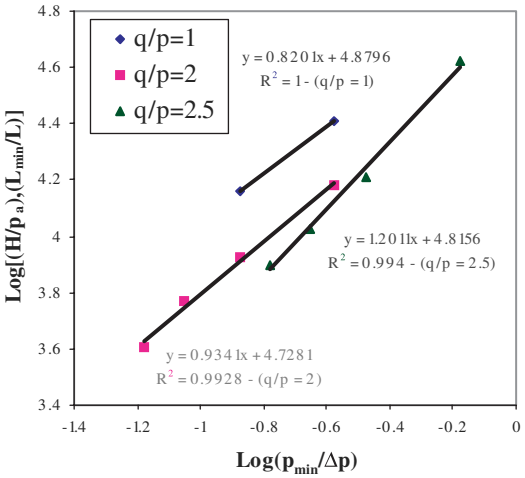

Figure 9. Evolution law of the hardening modulus for each q/p ratio.

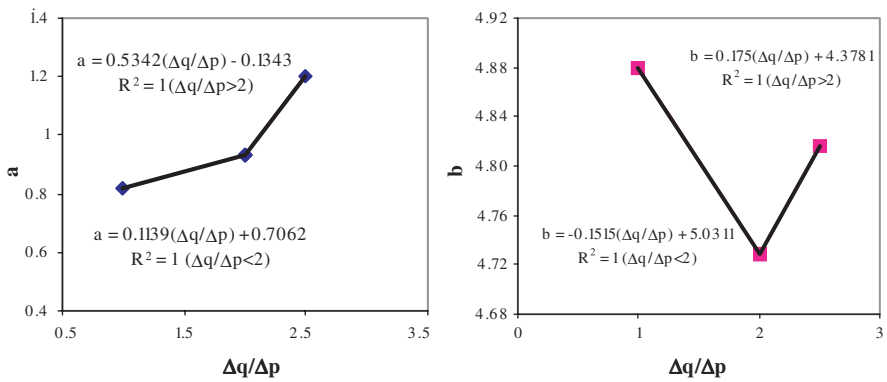

Figure 10. Variation of the parameters 'a' and 'b' with q/p for the Maraîchères UGM.

plane (Figure 11). Thus, we can express

$$B = \frac{L}{L_{\min}} \cdot \left(d + c \cdot \frac{p_{\min}}{\Delta p} \right) \tag{29}$$

where c and d are material parameters. These two parameters are defined with linear regression functions of the q/p ratio (Figure 12).

4. MODEL CALIBRATION WITH REPEATED LOAD TRIAXIAL TESTS

Figure 13 presents the typical response of the model when a loading and an unloading are performed, for a triaxial stress path. The cycle is described very simply; nevertheless, the expressions of the

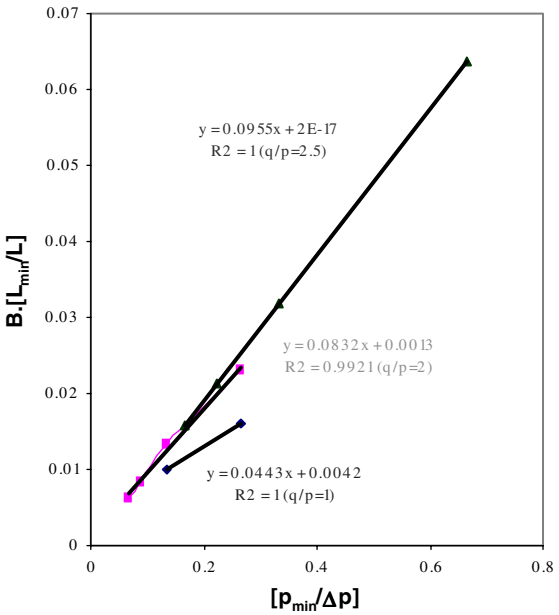

Figure 11. Evolution law of parameter 'B'.

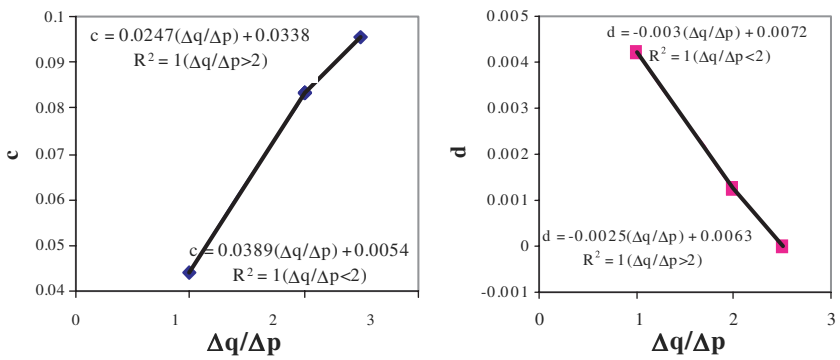

Figure 12. Variation of parameters c and d with q/p for the Maraîchères ($w = 4\%$).

yield surface and plastic potential take into account the influence of the stress path length and of the stress ratio (q/p) on the plastic strain at the end of unloading. This model is not able to describe accurately the loading–unloading cycle, but it can reproduce the axial plastic strain evolution under large cycle numbers.

The multi-stage repeated load triaxial tests, used to characterize the permanent deformations, have been modelled with the finite element code CAST3M [26] and Figure 14 shows a comparison between the computed plastic axial strains and the experiments, for the water content $w = 4\%$. The model predicts quite well the results obtained for the different stress paths $q/p = 1$, 2 and 2.5.

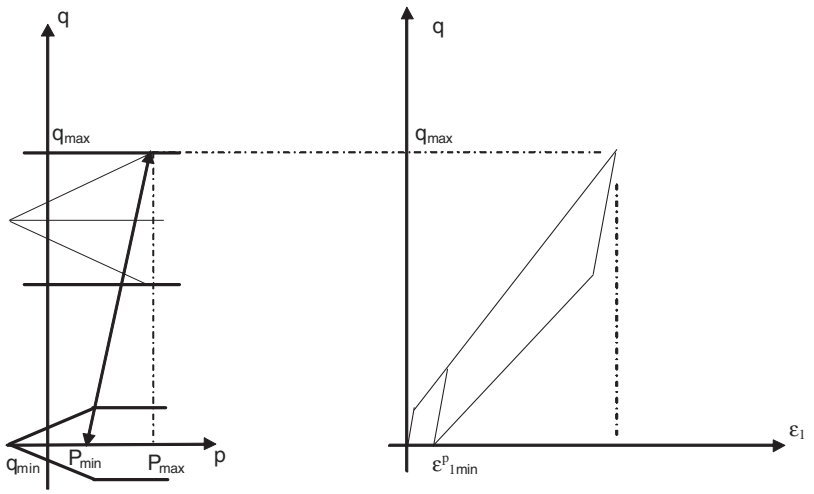

Figure 13. Evolution of the shape of the yield surface, plastic potential and typical stress—strain curve for a loading and an unloading cycle (triaxial test).

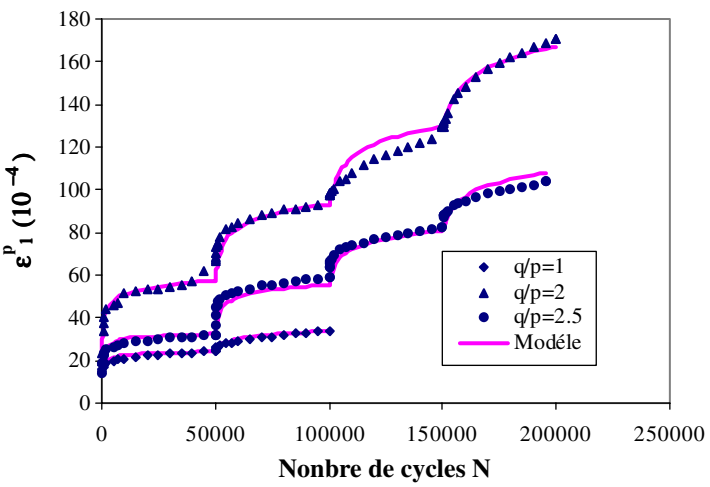

Figure 14. Comparison between the model and the experimental results (Maraîchères $w = 4\%$), stress path ratios $q/p = 1$, 2 and 2.5.

5. FINITE ELEMENT MODELLING OF A FULL-SCALE PAVEMENT STRUCTURE

5.1. Full-scale experiment

5.1.1. The LCPC-accelerated pavement testing facility. The LCPC-accelerated pavement testing facility, in Nantes, is an outdoor circular carousel dedicated to full-scale pavement experiments. The carrousel is composed of a central tower and four arms (20 m long) equipped with wheels,

Figure 15. View of the LCPC pavement testing facility.

running on a circular test track (see Figure 15). The tested circular pavement has a mean radius of 17.5 m, and thus a length of 110 m. The arms can be equipped with various load configurations: single or twinned wheels mounted on either a single or a tandem axle.

The machine can reach a maximum working speed of 15 rotations/min corresponding to a linear speed of about 100 km/h. Generally, for fatigue tests, the rotation speed is 10 rotations/ min (72 km/h) and then about one million loads can be applied to the pavement in one month. The lateral distribution of loads due to real traffic can be simulated during the rotations by a lateral wandering of the wheels, by steps of 10 cm, over a maximum width of 1.10 m.

The carousel is an outdoor equipment; hence, the pavements are submitted to normal climatic variations: rainfall, leading to variable moisture conditions in the unbound materials, and temperature variations.

5.1.2. Tested pavement structure. The experiment used in this work was performed in 2003. Four different low-traffic pavement structures with unbound granular bases were tested in this experiment. However, only one structure from this experiment will be analysed and modelled.

The selected pavement structure (Figure 16) consisted of the following:

- a 66 mm of asphalt surface layer;
- a 500 mm thick unbound granular base (Maraîchères granular material);
- a subgrade consisting of Missillac sand with a total thickness of 2200 mm.

The full-scale experiment involved the application of about two million loads between May and September 2003. The applied load was a 65 kN dual wheel load (32.5 kN per wheel), and the loading speed was 72 km/h. A lateral wandering was applied to the loads (distribution of the loads over 11 different lateral positions).

The experiment was performed in summer conditions, with low rainfall and temperatures in the asphalt layer varying mostly between 15 and 30°C. Typical moisture contents were $w = 4\%$ in the unbound granular layer and 8 % in the upper part of the soil, with little variations during the experiment.

To determine the parameters required for modelling the rutting of the pavement, complex modulus tests have been performed on the bituminous concrete and cyclic triaxial tests on the unbound materials. Their results have been described previously.

The pavement was instrumented (strain gage sensors, water content probes, thermocouples). Distress measurements were also performed at different stages of the experiment, including

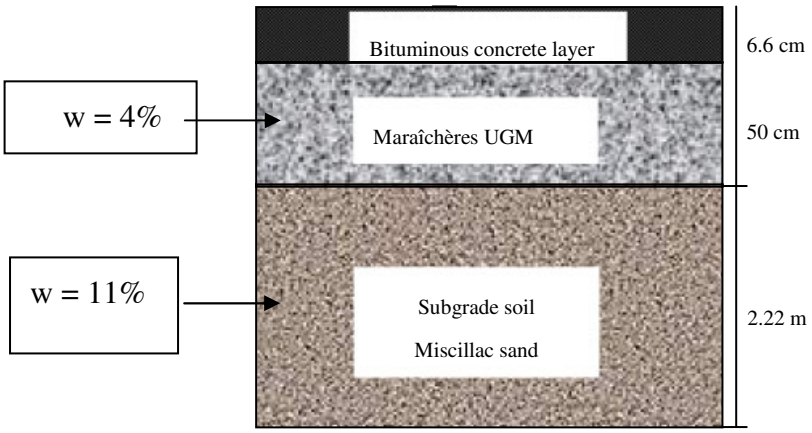

Figure 16. Low-traffic pavement studied with the LCPC pavement testing facility.

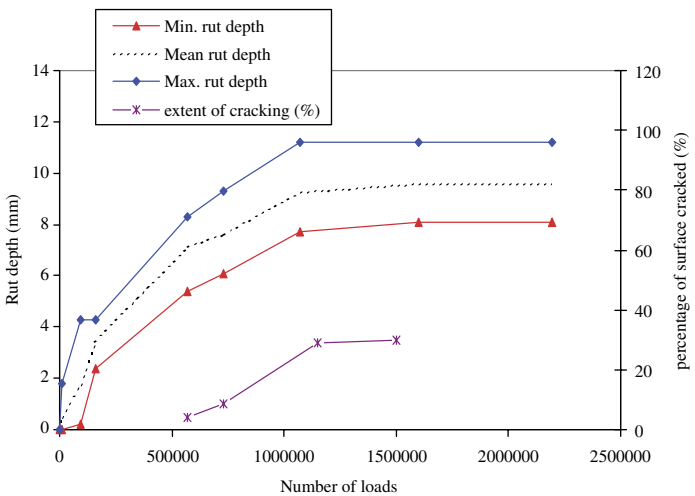

Figure 17. Evolution of rut depth and cracking on the experimental pavement.

measurements of the transversal profile of the pavement, to determine surface rutting (vertical deformations), and visual inspection, to determine surface cracking.

Figure 17 shows the evolution of the rutting of the pavement and also of the extent of surface cracking, with the number of applied loads. The results indicate that rutting was the main mode of distress of this pavement and was developed well before the apparition of the first cracks. Rutting increased rapidly at the beginning of the experiment, but tended to stabilize at the end of the experiment, at levels varying between 8 and 11 mm. This stabilization is probably due to the dry conditions towards the end of the experiment (practically no rainfall).

5.2. Finite elements modelling

The full-scale pavement structure was modelled with the simplified method in order to predict the rut depth evolution with time. The finite elements modelling with the finite elements code CAST3M involves three steps:

- The first step is the pre-processing where the finite elements mesh is generated, load and boundary conditions are assigned and material properties are defined.
- The second step is the elastic analysis where the minimum and the maximum stress fields are computed. We will see in Section 5.2.2 the procedure used to pass from the non-linear orthotropic elastic behaviour to the linear orthotropic elastic behaviour when finite elements modelling is performed.
- The third step is the calculation of the inelastic displacement and strain fields.

5.2.1. First step. For the calculations, the pavement is discretized into 20 noded cubical finite elements and 1000 elements have been used. Owing to the symmetry, the 3D calculation is carried out on a quarter of the structure (Figure 18).

The applied load is a 65 kN dual wheel load, corresponding to the standard axle load used in France for pavement design. The geometry of the contact area of the two wheels adopted in the calculations is represented in Figure 19. It corresponds to the contact area measured during the experiment.

The gravity and lateral stresses are first applied to the pavement structure to establish the initial *in situ* stress states (minimum load level). Such initial stresses are determined with the materials' unit weights and the lateral stress coefficient K_0, which is assumed to be equal to 0.5. Then the

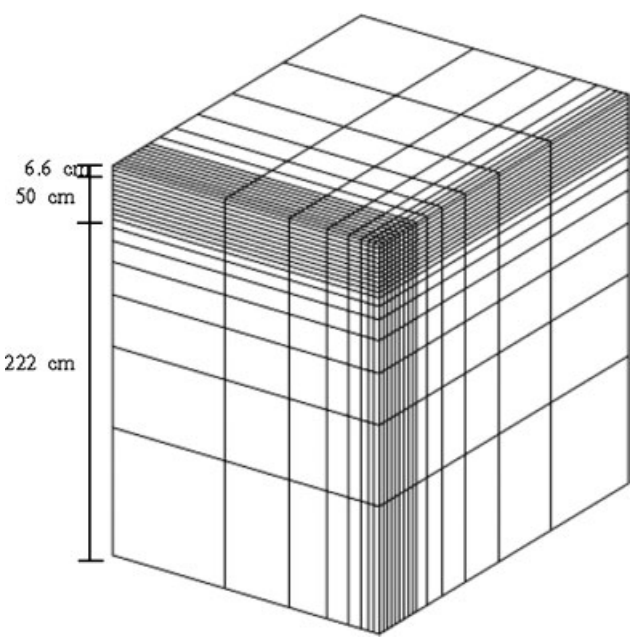

Figure 18. 3D Finite element mesh for pavement simulation.

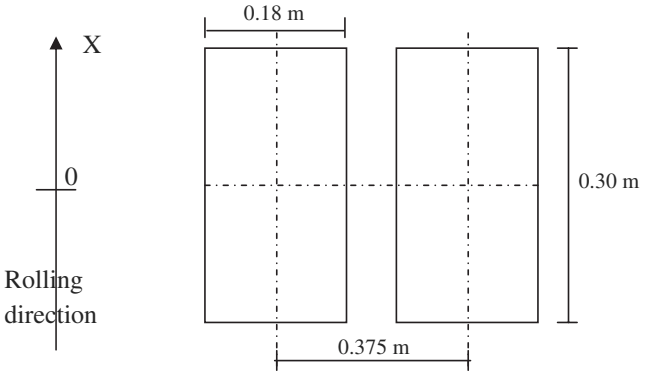

Figure 19. Modelling of the contact area of the dual wheel load (LCPC pavement testing facility).

pavement is subjected to the cyclic traffic loading (load described in Figure 19, with a maximum load level of 65 kN).

5.2.2. Second and third steps. The asphalt layer is considered homogeneous and an isotropic linear elastic model has been used with a Young modulus $E=6110\,\text{MPa}$ and a Poisson ratio $v=0.35$. The value of elastic modulus has been determined for values of frequency f and temperature T corresponding to the mean *in situ* conditions ($T=23°\text{C}$, $f=12.5\,\text{Hz}$).

For the granular layer and the subgrade, the non-linear orthotropic Boyce model has been used (material parameters defined in Table IV). It gives the maximum and minimum values of the stress fields, $S^{\text{el}}_{\min}(x)$ and $S^{\text{el}}_{\max}(x)$, respectively. To determine the linear elasticity matrix in (5)–(7) a secant calculation is carried out. It has been underlined in [27] that under the centre of a moving dual wheel load, where the maximum rut depth is obtained, the maximum deviation of the Lode angle is 20° (0° corresponds to a full shear state, whereas (−30°) and (30°) correspond to an extension (respectively, compression) triaxial stress state). Hence, the stress path under the centre of a moving dual wheel load can be considered as linear. We define the secant orthotropic shear and bulk modulus of the elasticity matrix M_{ijkl}:

$$\begin{aligned} K_{hh\Delta} &= \frac{p'_{\max}-p'_{\min}}{\varepsilon'_{v\max}-\varepsilon'_{v\min}}, \quad G_{hh\Delta}=\frac{q'_{\max}-q'_{\min}}{3(\varepsilon'_{d\max}-\varepsilon'_{d\min})} \\ E_{h\Delta} &= \frac{9G_{hh\Delta}K_{hh\Delta}}{3K_{hh\Delta}+G_{hh\Delta}}, \quad v_{hh\Delta}=\frac{3K_{hh\Delta}-2G_{hh\Delta}}{6K_{hh\Delta}+2G_{hh\Delta}} \\ E_{v\Delta} &= E_{h\Delta}/\gamma^2, \quad v_{hv\Delta}=\gamma\cdot v_{hh\Delta}, \quad G_{hv\Delta}=G_{hh\Delta}/\gamma \end{aligned} \tag{30}$$

with

$$\begin{aligned} p' &= \frac{\sigma_{xx}+\sigma_{yy}+\gamma\sigma_{zz}}{3}, \quad \varepsilon'_v=\varepsilon_{xx}+\varepsilon_{yy}+\varepsilon_{zz}/\gamma \\ q' &= \tfrac{1}{\sqrt{2}}\sqrt{(\sigma_{xx}-\sigma_{yy})^2+(\sigma_{xx}-\gamma\sigma_{zz})^2+(\sigma_{yy}-\gamma\sigma_{zz})^2+6(\sigma^2_{xy}+\gamma\sigma^2_{xz}+\gamma\sigma^2_{yz})} \\ \varepsilon'_d &= \tfrac{\sqrt{2}}{3}\sqrt{(\varepsilon_{xx}-\varepsilon_{yy})^2+(\varepsilon_{xx}-\varepsilon_{zz}/\gamma)^2+(\varepsilon_{yy}-\varepsilon_{zz}/\gamma)^2+6(\varepsilon^2_{xy}+\varepsilon^2_{xz}/\gamma+\varepsilon^2_{yz}/\gamma)} \end{aligned} \tag{31}$$

The structural transformed parameters field is determined using the maximum and minimum values of the stress fields, $S^{el}_{min}(x)$ and $S^{el}_{max}(x)$, respectively, of the elastic and plastic shakedown cases. Finally, the inelastic displacements and strain fields are determined with the parameters of the evolution law of the hardening modulus and of the function $F(N)$ for the Maraîchères material ($w=4\%$) and for the Miscillac sand ($w=11\%$).

5.3. Evolution of permanent deformations with the number of cycles and comparison experiment/calculation

Using the simplified method and the proposed evolution laws, the inelastic displacement and plastic strain fields can be calculated and compared with the results of the experiment.

On the pavement, the rut depth is measured on the pavement surface and includes the deformations of all pavement layers (bituminous layer, granular layer and subgrade). Five transversal rut profiles have been measured on the pavement, and from them, the minimum, mean and maximum values of the rut depth have been determined.

Four calculations have been carried out at 10^4, 10^5 and 10^6 load cycles and at the limit state. At each number of cycles, the calculation gives the mean value and range of the inelastic displacement and strain fields. Therefore, comparisons can be performed with the mean and maximum inelastic displacement field.

Figure 20 shows the shape of the rut depth profile obtained with the 3D analysis in the symmetry plane ($X=0\,$m), where the rut depth is maximum. It can be seen that the rut depth increases with increasing number of load applications and that the maximum rut depth is obtained at the centre of the dual wheel.

Figure 21 compares the calculated rut depth evolution (mean and maximum values) and the experiment (minimum, mean and maximum values). One can see that the simplified 3D finite element calculation is able to reproduce the final level of rutting but not the rut depth evolution with the number of load cycles. Several reasons could explain this result:

- The calculation does not take into account the lateral wandering of the loads applied in the experiment. The effect of the wandering leads to a shift of the experimental rut depth curve to the right and increases the difference with the calculation.

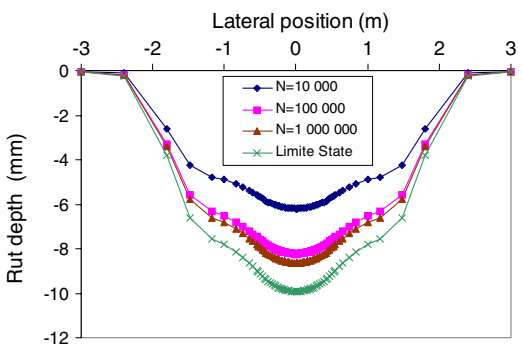

Figure 20. Calculation of the maximum rut depth cross profile.

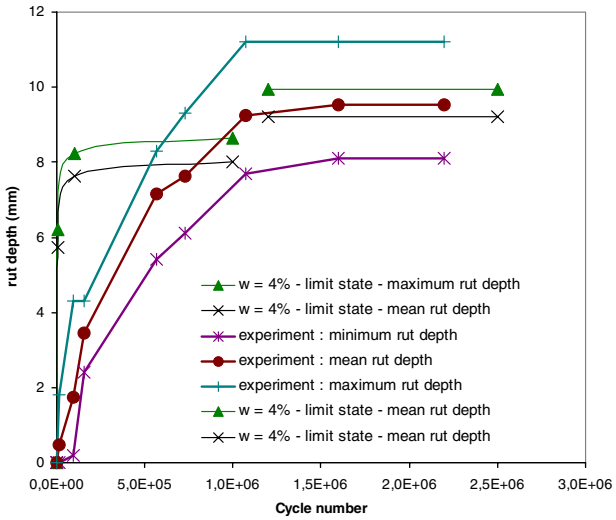

Figure 21. Comparison between the calculated rut depth and the experiment.

- The calculation is performed with constant, mean conditions of temperature and moisture and does not take into account the climatic variations. A better description of the variations of the Young modulus of the bituminous layer with temperature cycles and a better division of the base and subgrade layers taking into account the fluctuation of the water content could probably also improve the rut depth evolution.
- The calculation is performed under 'static' load conditions and does not take into account the loading due to the moving wheel. This type of loading induces stress rotations, which could have for effect an increase of the permanent deformations. A previous study performed by Hornych *et al.* [28] on an experimental pavement subject to both static loading (repeated plate load tests) and bi-directional moving wheel loading, has showed that moving loads produce higher deformations for the same maximum load level. However, taking into account stress rotation effects would also require appropriate laboratory tests, with stress rotation (such as hollow cylinder torsion tests), which are not available presently for unbound granular pavement materials.
- Finally, the model does not take into account dynamic effects due to the loading (speed 72 km/h). However, a 3D non-linear elastic calculation of the resilient behaviour of the pavement, where the elastic modulus of the bituminous layer is determined for a frequency corresponding to this speed (using the Huet and Sayegh model), and for the mean *in situ* temperature, shows that these hypotheses allow to reproduce correctly the deflections and resilient strains measured on the pavement (Figure 22).

It can be noted that the modelling results obtained here and the difference with the experimental results are very similar to those obtained by Suiker and de Borst [6], who made comparisons between a 2D finite elements calculation, performed with an equivalent visco-plastic model and a full-scale test on a railway track platform, also without taking into account the climatic variations. The comparisons between the predictions of the simplified shakedown model and those of the visco-plastic model with the same materials remain to be made.

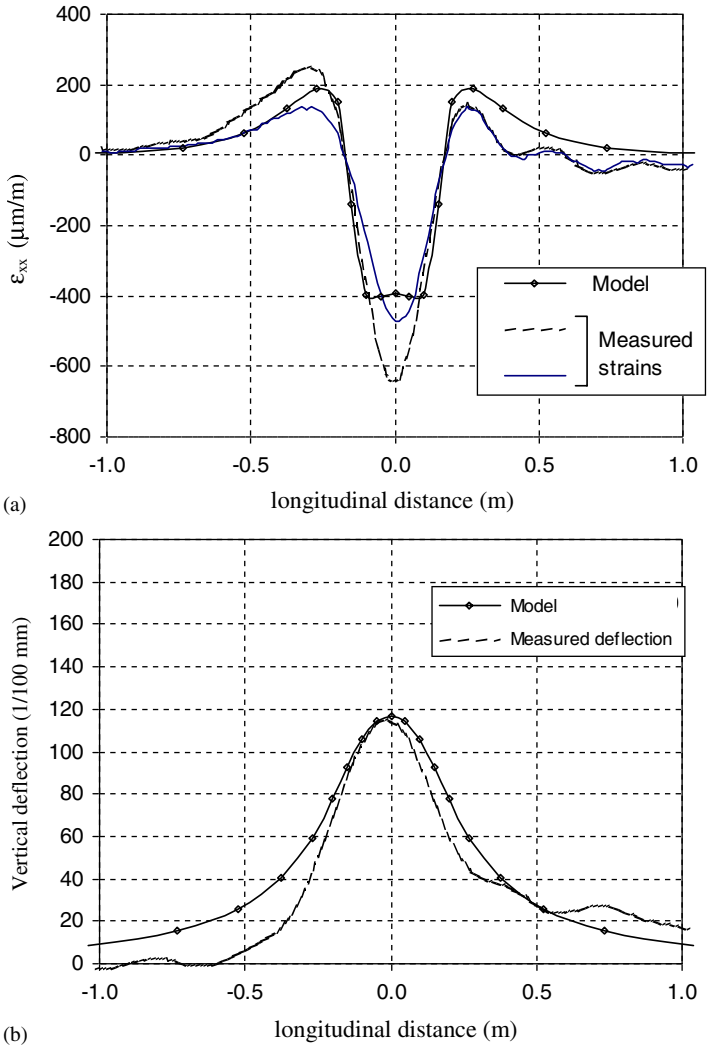

Figure 22. Comparison between measured resilient strains and displacements and modelling results: (a) longitudinal strains at bottom of bituminous layer and (b) vertical deflection.

The sensitivity of the model parameters to the test procedures used for the repeated load triaxial tests has been analyzed in [27] and the following results have been obtained:

- The influence of the number of loading stages, applied for parameter identification, on the vertical permanent deformation, is low (one or two percents), if at least three stages are applied, with maximum stress amplitudes close to the *in situ* stress amplitudes.
- The influence of the number of stress paths, applied for parameter identification, on the vertical permanent deformation, is low (one or two percents), if at least the following stress ratios are used: q/p=1, 2 and 3.

The influence of the number of stages and the number of stress paths required for parameter identification on the rut depth is low, if the previous remarks are taken into account.

Conversely, a factor that has a strong influence on the model parameters and, therefore, on the rut depth predictions is the water content of the material. Therefore, a good knowledge of the *in situ* water contents is important for the accuracy of the rut depth predictions. For instance, calculations performed in [27] have shown that the macroscopic cohesion introduced in the elastic calculation to take into account effect of unsaturated conditions can change the predicted rut depth by 30% compared with the calculation without cohesion.

6. CONCLUSION

This paper presents a simplified model for the prediction of rutting of unbound materials in low-traffic pavement. It requires four elasticity parameters for the orthotropic Boyce model and four plasticity parameters. The model parameters are determined from repeated load triaxial tests. The elasticity parameters are determined with the experimental procedure used to study the resilient behaviour and the knowledge of the macroscopic cohesion. The plasticity parameters require the determination of the hardening modulus. Then, the evolution law of the hardening modulus and the temporal function F are determined with the calculation of the stabilized plastic strain, which requires at least three permanent deformation tests, performed using a multi-stage procedure (application of several increasing stress levels, following the same stress path, with a constant q/p ratio).

The simplified calculation method, with statically admissible stress field and kinematically admissible strain field, is presently the most efficient way to perform 3D finite element calculations with large numbers of load cycles. Incremental step-by-step calculations would require accelerated calculation procedures, which have not been developed yet.

The simplified calculation method has been used to predict the rutting of an experimental pavement. The results obtained are encouraging and are a first step towards understanding the mechanisms of development of rutting in unbound pavement layers, although the simplified method does not take into account:

- variations of temperature, which modify the Young modulus of the asphalt layer, and of moisture content, which modify the elastic properties and the resistance to rutting of the unbound materials.
- the rotation of principal stress directions, which influences the elasto-plastic behaviour of the material.

Additional experiments and calculations are under way to test the Maraîchères material at higher water contents and to perform 3D finite element calculations with these new results. Further work is also planned to improve the rut depth prediction method, in particular,

- to take into account the influence of temperature on the mechanical behaviour of the bituminous material, with the knowledge of the number of cycles performed at a given temperature;
- to reduce the number of triaxial tests needed to study the mechanical behaviour of UGM. As testing at different water contents is very time consuming, an interpretation of the resilient behaviour and of the long-term behaviour with the effective stress concept could help to take into account the effect of moisture variations. Consequently, with the knowledge of the number of cycles performed at a given suction, the calculation of the rut depth could be improved.

Finally, other results of full-scale experiments, on instrumented pavements, will be needed to check the capabilities of the model to predict the behaviour of different types of pavement structures.

REFERENCES

1. Hicher PY, Daouadji A, Fegdouch D. Elastoplastic modelling of the cyclic behaviour of granular materials. *Proceedings of the International Workshop on Modelling and Advanced Testing for Unbound Granular Materials*, Lisbon, Balkema, Rotterdam, The Netherlands, 1999; 161–168.
2. Lekarp F, Dawson A. Modelling permanent deformation behaviour of UGM. *Construction and Building Materials* 1998; **12**(1):9–18.
3. Bonaquist RF, Witczak MW. A comprehensive constitutive model for granular materials in flexible pavement structures. *Proceedings of the 4th International Conference on Asphalt Pavements*, Seattle, Washington, U.S.A., 1997; 783–802.
4. Desai CS. Mechanistic pavement analysis and design using unified material and computer models. *Third International Symposium on 3D Finite Elements for Pavement Analysis,* Amsterdam, Balkema, The Netherlands, 2002; 1–63.
5. Chazallon C, Hornych P, Mouhoubi S. An elastoplastic model for the long term behaviour modelling of unbound granular materials in flexible pavements. *International Journal of Geomechanics* (ASCE) 2006; **6**(4):279–289.
6. Suiker ASJ, de Borst R. A numerical model for cyclic deterioration of railways tracks. *International Journal for Numerical Methods in Engineering* 2003; **57**:441–470.
7. Mayoraz F. Comportement mécanique des milieux granulaires sous sollicitations cycliques: application aux fondations des chaussées souples. Thèse de Doctorat, 2002, Ecole Polytechnique Fédérale de Lausanne.
8. Maier G, Pastor J, Ponter ARS, Weichert D. Direct methods of limit and shakedown analysis. In *Numerical and Computational Methods*, Chapter 12, vol. 3, de Borst R, Mang HA (eds). Elsevier/Pergamon: Amsterdam, 2003.
9. Zarka J, Casier J. Elastic plastic response of structure to cyclic loading: practical rules. *Mechanics Today*, vol. 6, Nemat-Nasser S (ed.). Pergamon Press: Oxford, 1979; 93–198.
10. Habiballah TM, Chazallon C. Cyclic plasticity based model for the unbound granular materials permanent strains modelling of flexible pavements. *International Journal for Numerical and Analytical Methods in Geomechanics* 2005; **29**:577–596.
11. Yu HS. Special issue on the Shakedown theory. *International Journal of Road Materials and Pavement Design* 2005; **6**:1.
12. Allou F, Chazallon C, Hornych P. A numerical model for flexible pavements rut depth evolution with time. *International Journal for Numerical and Analytical Methods in Geomechanics* 2007; **31**:1–22.
13. El Abd A. Développement d'une méthode de prédiction des déformations de surface des chaussées à assises non traitées. *Thèse de doctorat*, Université de Bordeaux, France, 2006.
14. Melan E. Theorie statisch unbestimmter systeme aus ideal-plastischem, Baustoff. *Sitzungsberichte Akademie Der Wissenschaften in Wien* 1936; **IIA**(195):145–195.
15. Mandel J. Généralisation de la théorie de plasticité de W.T. Koiter. *International Journal of Solids and Structures* 1965; **1**(3):273–296.
16. Halphen B, NGuyen QS. Sur les matériaux standards généralisés. *Journal of Mechanic* 1975; **14**(1):39–63.
17. Huet C. Etude par une méthode d'impédance du comportement visco-élastique des matériaux hydrocarbonés. *Thèse de Docteur-Ingénieur*, Faculté des Sciences de Paris, France, 1963.
18. Sayegh G. Contribution à l'étude des propriétés visco-élastiques des bitumes purs et des bétons bitumineux. *Thèse de Docteur-Ingénieur*, Sorbonne, France, 1965.
19. Hornych P, Kazai A, Piau JM. Study of the resilient behaviour of unbound granular materials. *Proceedings 5th Conference on Bearing Capacity of Roads and Airfields*, vol. 3, Trondheim, 1998; 1277–1287.
20. COST 337. Unbound granular materials for road pavements. European Commission Editon, Final report, 2003.
21. Boyce JR. A non linear model for the elastic behaviour of granular materials under repeated loading. *International Symposium on Soils under Cyclic and Transient Loading*, Swansea, 1980; 285–294.
22. Paute JL, Hornych P, Benaben JP. Comportement mécanique des graves non traitées. *Bulletin de Liaison des LPC* 1994; **190**:27–38.
23. Moreau JJ. Rafle par un convexe variable. *Séminaire Unilatérale*, Montpellier, France, 1971.
24. Hornych P, Corté JF, Paute JL. Etude des déformations permanentes sous chargements répétés de 3 graves non traitées. *Bulletin de Liaison des LPC* 1993; **184**:45–55.

25. Gidel G, Hornych P, Chauvin J-J, Breysse D, Denis A. Nouvelle approche pour l'étude des déformations permanentes des graves non traitées à l'appareil triaxial à chargement répétés. *Bulletin de liaison des Laboratoire des Ponts et Chaussées* 2001; **233**:5–22.
26. CAST3M. http://www-cast3m.cea.fr/cast3m, 2004. CAST3M is a research FEM environment; its development is sponsored by the French Atomic Energy Commission.
27. Chazallon C. Modélisation du comportement mécanique des milieux granulaires soumis à de grands nombres de sollicitations cycliques lentes. Application aux structures de chaussées à faible trafic. *HDR Dissertation*, Université Limoges, France, 2006 (in French).
28. Hornych P, KazaÏ A, Quibel A. Modelling a full scale experiment on two flexible pavements with unbound granular bases. *UNBAR5*, *5th International Symposium on Unbound Aggregates in Roads*, Nottingham, Balkema, Rotterdam, 2000; 359–367.